Proceedings of IMECE2008
2008 ASME International Mechanical Engineering Congress and Exposition
October 31-November 6, 2008, Boston, Massachusetts, USA

IMECE2008-68792

AXIALLY COMPRESSED CYLINDRICAL SHELLS CONTAINING ASYMMETRIC RANDOM IMPERFECTIONS: FOURIER SERIES TECHNIQUE AND ASME SECTION VIII DIVISION 1 AND 2 RULES

Gurinder Singh Brar*
University of North Carolina at Charlotte
9201 University City Blvd.
Charlotte, NC 28223-0001 USA
Tel: 704-808-0036 Fax: 704-687-6069
Email: gsbrar@uncc.edu
*Corresponding Author

Yogeshwar Hari
University of North Carolina at Charlotte
9201 University City Blvd.
Charlotte, NC 28223-0001 USA
Email: hari@uncc.edu

Dennis K. Williams
Sharoden Engineering Consultants, P.A
P.O. Box 1336
Matthews, NC 28106-1336 USA
Email: DennisKW@sharoden.com

ABSTRACT

This paper presents the comparison of reliability technique that employ Fourier series representations of random asymmetric imperfections in axially compressed cylindrical shell with evaluations prescribed by ASME Boiler and Pressure Vessel Code, Section VIII, Division 1 and 2. The ultimate goal of the reliability type technique is to predict the buckling load associated with the axially compressed cylindrical shell. Initial geometric imperfections have significant effect on the load carrying capacity of asymmetrical cylindrical shells. Fourier decomposition is used to interpret imperfections as structural features can be easily related to the different components of imperfections. The initial functional description of the imperfections consists of an axisymmetric portion and a deviant portion appearing as a double Fourier series. The representation of initial geometrical imperfections in the cylindrical shell requires the determination of appropriate Fourier coefficients. The mean vector and the variance-covariance matrix of Fourier coefficients are calculated from the simulated shell profiles. Multi-mode analysis are expanded to evaluate a large number of potential buckling modes for both predefined geometries and associated asymmetric imperfections as a function of position within a given cylindrical shell. Large number of shells thus created can be used to calculate buckling stress for each shell. The probability of the ultimate buckling stress exceeding a predefined threshold stress can also be calculated.

Keywords: Buckling; Asymmetric Imperfections; Fourier Series; Cylindrical Shell.

NOMENCLATURE

λ = Non-dimensional buckling load
μ = Poisson's ratio
ξ_i = Magnitude of imperfection as a fractional value of shell thickness
θ = Non-dimensional number associated with the circumferential coordinates
ξ = Non-dimensional number associated with the axial coordinates
$\sigma_A(\xi)$ = Elements of Variance-covariance matrix
$C_{w0}(\xi_1,\theta_1,\xi_2,\theta_2)$ = Auto-covariance function
k = Number of half waves in axial direction
l = Number of full waves in circumferential direction
P_{cl} = Classical buckling load of a perfect shell
P_{cr} = Critical buckling load of a shell with imperfections

R = Radius of the shell
E = Young's Modulus
L = Length of the shell
t = Wall thickness of the shell
D_0 = Outside diameter of the shell
$W_n(\xi,\theta)$ = Initial imperfection function

INTRODUCTION

Buckling is failure of a member under compression. Buckling is characterized by the appearance and growth of bulges, ripples or waves. It is usually encountered in thin structural members when they show visibly large transverse displacement to the applied load. Buckling strength of thin cylindrical shells is influenced by the initial imperfection in the geometry of the cylindrical shell. Cylindrical shell having variations in the wall thickness as imperfection is studied in this paper.

The classical buckling load of a perfect shell can be calculated by eq. (1) as given by Fung and Sechler [1] and Amazigo and Budiansky [2]. The assumption for eq. (1) to hold true is that cylindrical shell; with perfect elasticity, initial shape and uniform wall thickness, is under compressive load fixed in axial direction and load is uniformly distributed along the circumference.

$$P_{cl} = \frac{E}{\sqrt{3(1-\mu^2)}}\frac{t}{R} \tag{1}$$

When imperfections in shells come into picture load carrying capacity of shells is reduced. Non-dimensional buckling load (λ) defined in eq. (2) is a factor that takes into accounts the effect of imperfections and determines the critical buckling load.

$$\lambda = \frac{P_{cr}}{P_{cl}} \tag{2}$$

The cylindrical shell under study is stack portion of the FGD vessel. The flue gas desulphurization (FGD) "vessel" is a large hybrid tank-vessel-stack assembly in a major Canadian refinery. The function of the FGD vessel is to contain and support a proprietary process that utilizes an ammonium sulphate scrubbing system to produce environmentally friendly air emissions. Waste ammonia is employed to scrub the air emissions, which eventually are discharged through a 6.1 m. diameter stack that extends approximately 94.2 m. above ground level. Within the hybrid FGD vessel and its associated components, slurry is processed from the scrubber whereby the final by-product of the process is a granular ammonium sulphate [3].

The overall absorber/stack assembly is shown in Fig. 1. Due to the vessel height of approximately 94.2 m., it is readily apparent that column-type instability must be considered in the design of the vessel. The FGD absorber/stack assembly is utilized in a petroleum refinery installation and is comprised of three major structural and geometric sections. The bottom section resembles (in many respects) an API Standard 650 storage tank [4] with its 21.3 m. diameter thin wall cylindrical construction as discussed by Williams [5]. The maximum internal design pressure of approximately 255 kPa in the storage tank portion is primarily attributed to the linearly varying hydrostatic load within the tank. The middle section of the FGD absorber/stack is comprised of both cylindrical and conical pressure vessels that are subjected to pressures ranging from –1.86 to 3.72 kPa. These intermediate sections are designed in accordance with the ASME Boiler and Pressure Vessel Code, Section VIII, Division 1 [6]. The third and upper most section is comprised of multiple ring-stiffened sections of decreasing wall thicknesses as a function of elevation and resembles an ASME STS-1 stack [7]. Because the height of the FGD absorber/stack exceeds 91.4 m. in combination with tank diameters of approximately 21.3 m., wind loads, self-weight, and platform loads become a significant consideration in the design of the entire assembly. The aforementioned dead and live loads create both tensile and compressive stresses that must be combined with the stresses associated with both positive and negative internal pressures along the length of the hybrid FGD absorber/stack [8]. The compressive stresses in the tall, slender portion of the FGD (i.e., the stack) are the most obvious motivating forces for considering a buckling type failure.

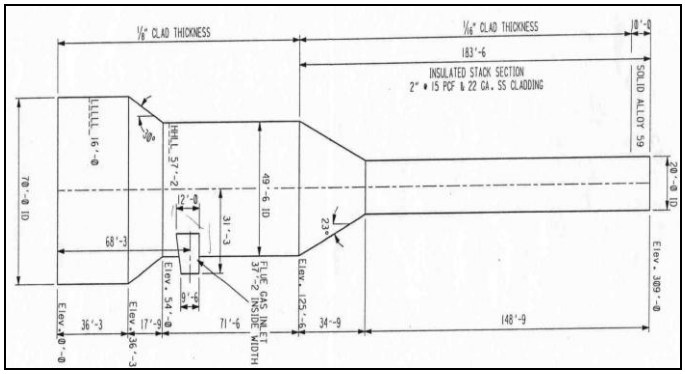

Fig. 1 FGD Vessel/Stack [8]

RELIABILITY OF AXIALLY LOADED CYLINDRICAL SHELL WITH ASYMMETRIC VARIABLE WALL THICKNESS

Solution of thin cylindrical shell containing small asymmetric thickness variations while subjected to an axial end load, the reliability approach employs the simulation of number of shells using Monte Carlo technique, calculation of buckling loads using Multimode analysis, and calculation of non-dimensional buckling load (λ) based on reliability function. Similar to the method described by Elishakoff et al. [9], any initial imperfection can be represented by series of cosines and sines. A review of the previously defined work [9] indicated numerous errors in the formulations and figures as published in the open literature, thereby creating the necessity to revisit the bases for the results as described by the authors [9]. With this in mind, as given by Elishakoff and Arbocz [10] and Arbocz and Williams [11], the initial imperfection function $\mathbf{W_n(\xi,\theta)}$ can be represented as shown in eq. (3):

$$W_n(\xi,\theta) = \sum_{i=0}^{N_1} a_i \cos(i\pi\xi) + \sum_{k=1}^{N_2}\sum_{l=1}^{N_3}\begin{bmatrix} b_{kl}\sin(k\pi\xi)\cos(l\theta) \\ +c_{kl}\sin(k\pi\xi)\sin(l\theta)\end{bmatrix} \tag{3}$$

The chosen coordinate system for the cylindrical shell utilizes axial (**x**) and circumferential (**y**) coordinates. In addition, $\mathbf{a_i}$, $\mathbf{b_{kl}}$, and $\mathbf{c_{kl}}$ are fourier coefficients of the respective terms. Eq. (4) gives the relation of non-dimensional numbers $\boldsymbol{\xi}$ and $\boldsymbol{\theta}$ with the axial and circumferential coordinates.

$$\xi = \frac{x}{L}, 0 \le x \le L$$
$$\theta = \frac{y}{R}, 0 \le \theta \le 2\pi \quad (4)$$

The length and radius of the cylindrical shell are represented by **L** and **R**. The first half range cosine series summation term in eq. (3) denotes the axisymmetric part of imperfection and second half range sine series summation term denotes the non-symmetric part. Equation (3) can also be written in a more simplified way as:

$$W_0(\xi,\theta) = \sum_{i=1}^{N_1} A_i \cos(i\pi\xi) + \sum_{r=1}^{N} \begin{bmatrix} C_r \sin(k_r\pi\xi)\cos(l_r\theta) \\ +D_r \sin(k_r\pi\xi)\sin(l_r\theta) \end{bmatrix} \quad (5)$$

The index, r is selected so that eq. (3) can be represented by eq. (5) and also $N = N_2 x N_3$.

The means of the fourier coefficients of **N** simulated shells is determined by eq. (6):

$$K_{A_iA_j}{}^{(e)} = \frac{1}{N-1}\sum_{m=1}^{N}\left(A_i^{(m)} - A_i^{(e)}\right)\left(A_j^{(m)} - A_j^{(e)}\right)$$

$$K_{C_rC_s}{}^{(e)} = \frac{1}{N-1}\sum_{m=1}^{N}\left(C_r^{(m)} - C_r^{(e)}\right)\left(C_s^{(m)} - C_s^{(e)}\right)$$

where,

$$A_i^{(e)} = \frac{1}{N}\sum_{m=1}^{N} a_i^{(m)}$$
$$C_r^{(e)} = \frac{1}{N}\sum_{m=1}^{N} c_r^{(m)} \quad (6)$$

The elements of variance-covariance matrix are calculated by eq. (7):

$$\sigma^2{}_A(\xi) = \sum_{i=0}^{N_1}\sum_{j=0}^{N_1} K_{A_iA_j}\delta_{ij}\cos(\pi i\xi)\cos(\pi j\xi)$$

$$\sigma^2{}_C(\xi,\theta) = \sum_{r=1}^{N}\sum_{s=1}^{N}\begin{bmatrix} K_{C_rC_s}\sin(k_r\pi\xi)\sin(k_s\pi\xi) \\ \cos(l_r\theta)\cos(l_s\theta) \end{bmatrix}$$

$$\sigma^2{}_D(\xi,\theta) = \sum_{r=1}^{N}\sum_{s=1}^{N}\begin{bmatrix} K_{D_rD_s}\sin(k_r\pi\xi)\sin(k_s\pi\xi) \\ \cos(l_r\theta)\cos(l_s\theta) \end{bmatrix} \quad (7)$$

The simulation process should be checked by the auto-covariance function of the simulated N shells. The auto-covariance function $\mathbf{C_{w0}(\xi_1,\theta_1,\xi_2,\theta_2)}$ is then calculated by eq. (8) and has to be compared to the auto-covariance function of the initial sample. The auto-covariance function gives a measure of linear association between two variables of the same process. The prefix 'auto' means a reflexive act on oneself, and thus auto-covariance is the covariance that the process has with itself.

Once the auto-covariance function of the simulated shells agrees with the actual shell and variance-covariance matrix has been investigated, the next step is to calculate buckling load for each simulated shell using Multi-mode analysis [12].

$$C_{w_0}(\xi_1,\theta_1;\xi_2,\theta_2) = \sum_{i=0}^{N_1}\sum_{j=0}^{N_1} K_{A_iA_j}\cos(i\pi\xi_1)\cos(j\pi\xi_2)$$
$$+\sum_{i=0}^{N_1}\sum_{s=1}^{N} K_{A_iC_s}\cos(i\pi\xi_1)\sin(k_s\pi\xi_2)\cos(l_s\theta_2)$$
$$+\sum_{i=0}^{N_1}\sum_{s=0}^{N} K_{A_iD_s}\cos(i\pi\xi_1)\sin(k_s\pi\xi_2)\sin(l_s\theta_2)$$
$$+\sum_{r=1}^{N}\sum_{j=0}^{N_1} K_{C_rA_j}\sin(k_r\pi\xi_1)\cos(j\pi\xi_2)\cos(l_r\theta_1)$$
$$+\sum_{r=1}^{N}\sum_{j=0}^{N_1} K_{D_rA_j}\sin(k_r\pi\xi_1)\cos(j\pi\xi_2)\sin(l_r\theta_1)$$
$$+\sum_{r=1}^{N}\sum_{s=1}^{N} K_{C_rC_s}\sin(k_r\pi\xi_1)\cos(l_s\theta_2)\sin(k_s\pi\xi_2)\cos(l_r\theta_1)$$
$$+\sum_{r=1}^{N}\sum_{s=1}^{N} K_{C_rD_s}\sin(k_r\pi\xi_1)\cos(l_r\theta_1)\sin(k_s\pi\xi_2)\sin(l_s\theta_2)$$
$$+\sum_{r=1}^{N}\sum_{s=1}^{N} K_{D_rC_s}\sin(k_r\pi\xi_1)\sin(l_r\theta_1)\sin(k_s\pi\xi_2)\cos(l_s\theta_2)$$
$$+\sum_{r=1}^{N}\sum_{s=1}^{N} K_{D_rD_s}\sin(k_r\pi\xi_1)\sin(l_r\theta_1)\sin(k_s\pi\xi_2)\sin(l_s\theta_2) \quad (8)$$

The auto-covariance function $\mathbf{C_{w0}(\xi_1,\theta_1,\xi_2,\theta_2)}$ can be written in simplified form as:

$$C_{w_0}(\xi_1,\theta_1,\xi_2,\theta_2) = \sum_{i=0}^{N_1}\sum_{j=0}^{N_1} K_{A_iA_j}\cos(i\pi\xi_1)\cos(j\pi\xi_2)$$
$$+\sum_{r=1}^{N}\sum_{s=1}^{N} K_{C_rC_s}\sin(k_r\pi\xi_1)\sin(k_s\pi\xi_2)\cos(l_r(\theta_2-\theta_1)) \quad (9)$$

The critical buckling loads for N simulated shells can be represented in a reliability v/s non-dimensional buckling load plot and critical non-dimensional buckling load at desired reliability can be calculated as given in Elishakoff [13]. Also, absolute difference between calculated value and theoretical value can be calculated according to Kolmogorov-Smirnov test of goodness of fit as given by Massey [14].

SIMULATION OF CYLINDRICAL SHELLS

The cylindrical shell under study is the upper part of FGD vessel or stack. FGD vessel stack has internal diameter of 6.1m, height of 7.9248m and wall thickness of 9.525mm (0.375in.). The various dimensions and properties of FGD stack are shown in Table 1 below:

Table 1 Technical Specifications of FGD Stack Shell

Property	Value
Shell Wall Thickness, t	3/8 in.
Length of Stack, L	312 in.
Radius of Shell, R	120 in.
Young's Modulus, E	3 x 10^7 psi
Poisson's Ratio, μ	0.31

Initial imperfections in FGD vessel are in the form of wall thickness variations. For calculation of buckling load, 50 cylindrical shells (GB1-GB50) were simulated using MathCAD code. The code utilizes linear congruence method for generation of random numbers. As per the ASME standards [6], "The reduction in thickness shall not exceed 1/32 in. (1mm) or 10% of the nominal thickness of the adjoining surface, whichever is less". Therefore, shell wall thickness varies between 0.375in. and 0.344in. Total 144 readings were generated for each shell, 12 readings axially and 12 circumferentially at each elevation. Table 1 in APPENDIX displays generated shell wall thickness values for GB8 Shell.

The shell wall thickness values thus generated represent asymmetric imperfection and can be converted into axisymmetric imperfections by taking arithmetic mean of all values at a particular elevation. Fig. 2 and Fig. 3 shows the asymmetric and axisymmetric variations in shell wall thickness value for GB8 Shell respectively.

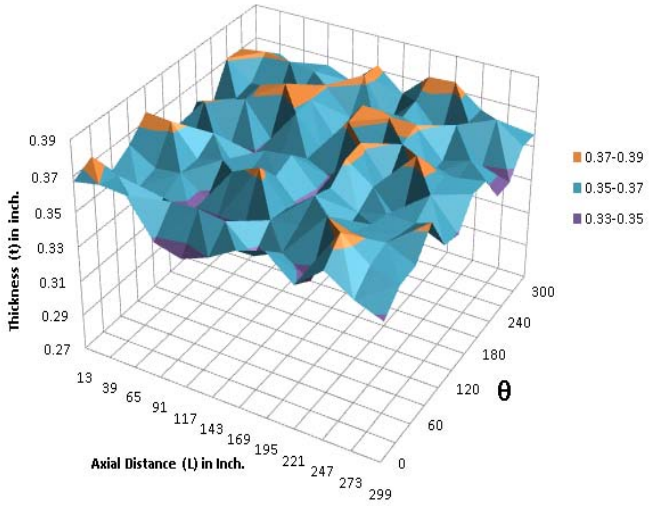

Fig. 2 Asymmetric variation of Shell Wall Thickness for GB8 Shell

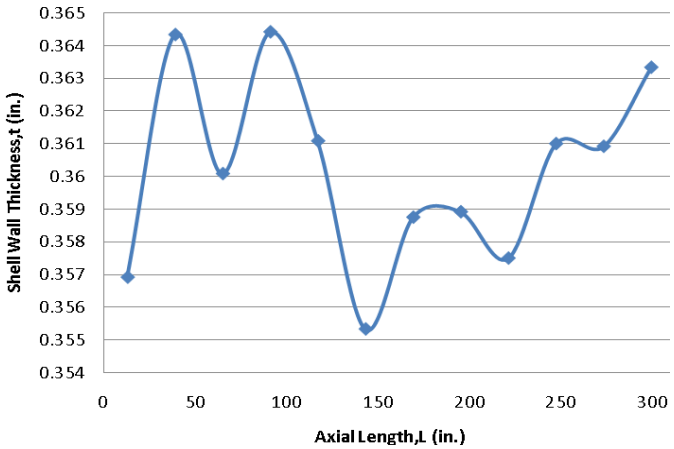

Fig. 3 Axisymmetric variation of Shell Wall Thickness for GB8 Shell

The initial asymmetric imperfections are represented by eq. (5) and fourier coefficients were calculated. Table 2 in APPENDIX shows first eleven fourier coefficients for GB Shells. Then sample mean was calculated using eq. (6). The elements of variance-covariance matrix were calculated from eq. (7) and are shown in Table 3 in APPENDIX. For 25 GB Shells variance-covariance matrix comes out to be matrix of 25X25. As can be seen from the matrix the maximum peaks are at the diagonal elements and as one moves away from the diagonal elements the peaks vanishes.

The auto-covariance function which gives the measure of linear association between two variables was calculated by eq. (9) using MathCAD code. Fig. 4 shows the auto-covariance function for GB Shells. The plot is non-uniform and thus concludes that the initial imperfections of GB shells make up non-homogenous random fields.

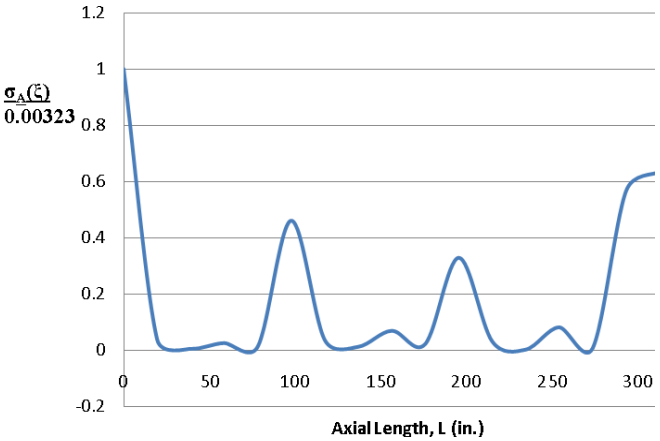

Fig. 4 Auto-covariance Function for GB Shells

CALCULATION OF BUCKLING LOADS

Buckling loads for 50 GB Shells was calculated using Multi-mode method [12] using MathCAD code. A column plot showing number of buckled shells for specific values of non-dimensional buckling load (λ) are shown in Fig. 5. This plot will be used for calculating the reliability function from which experimental value of non-dimensional buckling load can be calculated.

Fig. 6 shows the reliability function for 50 GB Shells. The value of non-dimensional buckling load (λ) can be calculated at any desired reliability from this curve. If the desired reliability is 0.95, then the non-dimensional buckling load (λ) comes to be 0.780. Depending on the sample size, there is difference in obtained value and theoretical value. From Table 1 of Massey [14] it can be concluded that for 50 sample size and 0.05 level of significance, absolute difference between calculated and theoretical value is 0.19. So, the value of non-dimensional buckling load (λ) comes to be (0.780-0.19) that is 0.590.

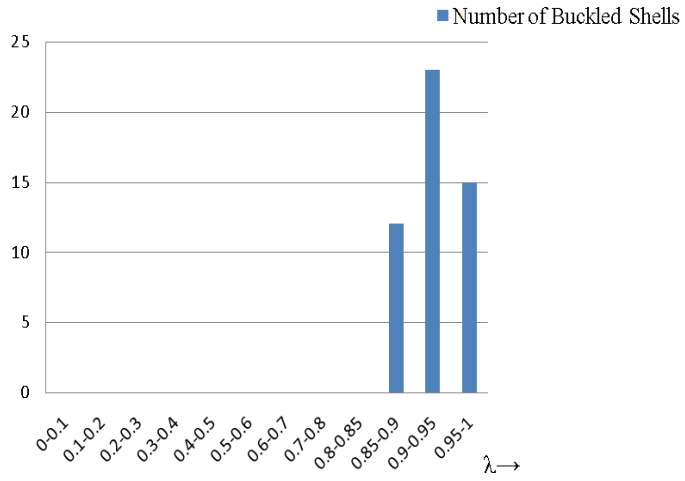

Fig. 5 Non-dimensional Buckling Loads for 50 GB Shells

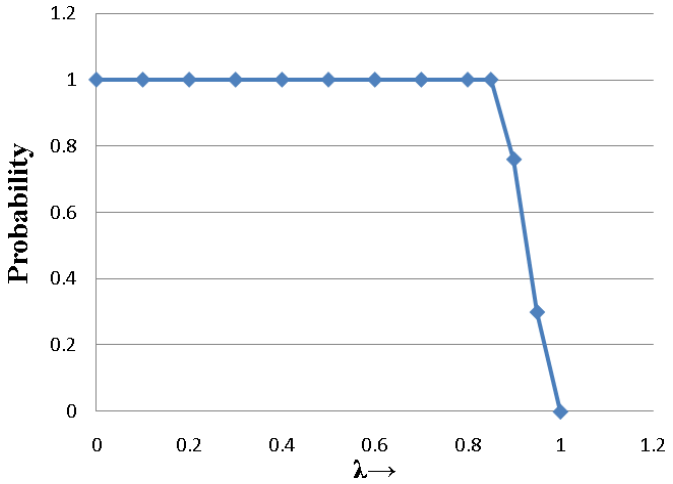

Fig. 6 Calculated Reliability Function V/S Non-dimensional Buckling Load

As per ASME [6], capacity reduction factors (β) that accounts for shape imperfections must be applied to the allowable stresses. Eq. (10) is used to calculate the capacity reduction factor for unstiffened cylinders.

$$\beta = 0.207 \; for \; \frac{D_0}{t} \geq 1247$$
$$\beta = \frac{338}{389 + \frac{D_0}{t}} \; for \; \frac{D_0}{t} < 1247 \qquad (10)$$

The ratio D_0/t for FGD Stack comes out to be 322. Thus, using eq. (10) the value of β comes out to be 0.475.

RESULTS AND CONCLUSIONS

The classical buckling load for FGD vessel by eq. (1) comes out to be 56.75ksi. This load carrying capacity will be reduced due to presence of imperfections. The results obtained from the evaluation of non-dimensional buckling load by Monte Carlo technique and ASME code leads to Table 2. These results show that the effect of shell wall thickness variation on buckling load deserves special attention. Thus, in the absence of initial geometric imperfection, this particular kind of thickness variation may constitute the most important factor in the buckling load reduction. In this situation, non-dimensional buckling load (λ) comes out to be 0.590 by Monte Carlo technique. It means that due to presence of shell wall thickness variation as a result of non-repeatability in manufacturing process even within tolerance limits, the load carrying capacity of shell decreases by 41%. Thus it can be concluded that imperfections in shell wall thickness have been addressed in ASME code by capacity reduction factor. The results obtained by Monte Carlo method agree well with those published by Elishakoff et al. [9] for the prediction of buckling load.

Table 2 Buckling Loads for FGD vessel

Buckling Loads derived for Axisymmetric buckling mode	
ASME Code	0.475
Monte Carlo Technique	0.590

REFERENCES

1. Fung, Y. C., and Sechler, E. E., "Instability of Thin Elastic Shells", *First Symposium on Naval Structural Mechanics (edited by J. Norman Goodier and N. J. Hoff),* Pergamon Press, New York, 115-68, 1960.
2. Amazigo, J. C., and Budiansky, B., "Asymptotic Formulas for the Buckling Stresses of Axially Compressed Cylinders with Localized or Random Axisymmetric Imperfections," *Journal of Applied Mechanics*, 39, 179-84, 1972.
3. Marsulex, 2003, "2003 Annual Meeting: 2002 Operating Review," www.marsulex.com, Toronto, Ontario.
4. API, 1998, *Welded Steel Tanks for Oil Storage, API Standard 650, Tenth Edition*, November 1998, American Petroleum Institute, Washington, DC.
5. Williams, D. K., 2004, "Buckling Considerations and the Use of Code Case 2286-1 for Analyzing a Flue Gas Desulphurization Vessel," *Design & Analysis of Pressure Vessels, Heat Exchangers & Piping Components*, ASME PVP Vol. 477, New York.
6. ASME, 2001, *ASME Boiler & Pressure Vessel Code, Section VIII, Division 1*, American Society of Mechanical Engineers, New York.
7. ASME, 2000, *ASME STS-1-2000, Steel Stacks*, American Society of Mechanical Engineers, New York.
8. Dennis K, Williams, James R. Williams, Yogeshwar Hari., "Buckling of Imperfect Axisymmetric Homogeneous Shells of Variable Thickness: Perturbation Solution", *International Conference & Exhibition on Pressure Vessels and Piping* "OPE 2006 – CHENNAI" February, 7-9, 2006, Chennai, India.
9. Elishakoff, I., Li, Y., and Starnes, J. H., Jr., 2001, *Non-Classical Problems in the Theory of Elastic Stability*, Cambridge University Press, Cambridge, UK.
10. Elishakoff, I., and Arbocz, J., "Reliability of Axially Compressed Cylindrical Shells with General Non-symmetric Imperfections," *Journal of Applied Mechanics*, Vol. 52, 122-8, 1985.
11. Arbocz, J., and Williams, J. G., "Imperfection Surveys on a 10-ft Diameter Shell Structure," *AIAA Journal,* Vol. 15, No. 7, 949-56, July, 1977.
12. Arbocz, J., and Babcock, C. D., Jr., "A Multi-Mode Analysis for Calculating Buckling Loads of Imperfect Cylindrical Shells," GALCIT Report SM-74-4, California Institute of Technology, Pasadena, California, June, 1974.
13. Elishakoff, I., "Buckling of a Stochastically Imperfect Finite Column on a Nonlinear Elastic Foundation – A Reliability Study," *Journal of Applied Mechanics*, Vol. 46, 411-6, June, 1979.
14. Massey, F. J., Jr., "The Kolmogorov-Smirnov test for goodness of fit," *Journal of American Statistical Assessment*, Vol. 46, 68-78, 1951.

APPENDIX

Table 1 Shell Wall Thickness of GB8 Shell

θ\L(in.)	13	39	65	91	117	143	169	195	221	247	273	299
0	0.370	0.374	0.367	0.361	0.374	0.363	0.357	0.368	0.350	0.363	0.350	0.346
30	0.374	0.358	0.357	0.361	0.356	0.363	0.363	0.374	0.361	0.372	0.368	0.373
60	0.365	0.352	0.350	0.361	0.368	0.372	0.355	0.359	0.365	0.344	0.365	0.375
90	0.355	0.373	0.345	0.373	0.351	0.372	0.346	0.350	0.349	0.370	0.348	0.374
120	0.366	0.361	0.356	0.373	0.347	0.361	0.350	0.369	0.371	0.362	0.364	0.367
150	0.362	0.352	0.348	0.359	0.353	0.350	0.349	0.364	0.363	0.374	0.367	0.368
180	0.350	0.366	0.366	0.364	0.351	0.355	0.370	0.371	0.374	0.358	0.370	0.365
210	0.369	0.349	0.358	0.365	0.347	0.358	0.352	0.351	0.375	0.362	0.357	0.350
240	0.360	0.352	0.366	0.356	0.361	0.367	0.374	0.361	0.356	0.349	0.372	0.355
270	0.361	0.350	0.355	0.375	0.349	0.368	0.350	0.357	0.364	0.373	0.373	0.367
300	0.364	0.367	0.349	0.350	0.369	0.356	0.358	0.372	0.370	0.346	0.347	0.347
330	0.357	0.355	0.369	0.372	0.369	0.362	0.364	0.371	0.351	0.349	0.359	0.346
Mean	0.3628	0.3591	0.3572	0.3642	0.3579	0.3623	0.3573	0.3639	0.3624	0.3602	0.3617	0.3611

Table 2 Fourier Coefficients (A_i) for GB Shells

a_i	GB1	GB2	GB3	GB4	GB5	GB6	GB7	GB8	GB9	GB10	GB11	GB12	GB13
0	0.36000	0.35756	0.36006	0.36006	0.35939	0.35876	0.36081	0.36022	0.35897	0.35863	0.35949	0.35898	0.35881
1	0.00085	0.00002	-0.00054	0.00111	0.00155	-0.00012	-0.00132	0.00010	0.00056	-0.00015	0.00005	0.00336	0.00001
2	0.00045	-0.00079	0.00111	-0.00006	-0.00098	-0.00097	0.00007	0.00157	-0.00121	-0.00099	0.00071	0.00112	-0.00147
3	0.00024	0.00042	-0.00019	0.00052	0.00013	-0.00026	0.00049	-0.00184	0.00105	0.00077	-0.00072	-0.00102	0.00001
4	-0.00033	-0.00150	-0.00225	-0.00081	-0.00017	0.00182	0.00124	-0.00120	-0.00016	-0.00027	-0.00007	-0.00138	-0.00071
5	-0.00026	0.00032	-0.00003	0.00051	0.00230	0.00073	0.00013	-0.00099	0.00124	0.00034	-0.00047	-0.00024	-0.00002
6	0.00207	0.00122	-0.00120	-0.00045	0.00196	-0.00253	-0.00133	0.00017	-0.00003	0.00037	0.00059	-0.00001	0.00036
7	0.00063	-0.00044	-0.00144	0.00091	0.00028	0.00030	-0.00020	0.00027	0.00198	0.00044	-0.00112	-0.00154	0.00132
8	-0.00073	0.00028	0.00150	-0.00149	-0.00010	0.00030	-0.00039	-0.00092	0.00023	0.00049	0.00043	0.00039	0.00143
9	-0.00030	-0.00047	0.00096	0.00059	-0.00055	-0.00055	-0.00005	-0.00171	-0.00013	-0.00011	0.00020	0.00110	0.00053
10	-0.00072	0.00101	-0.00035	-0.00092	0.00030	0.00058	-0.00138	-0.00035	0.00053	-0.00147	0.00012	-0.00056	-0.00016
a_i	GB14	GB15	GB16	GB17	GB18	GB19	GB20	GB21	GB22	GB23	GB24	GB25	Mean (A_i)
0	0.35943	0.36008	0.35993	0.35996	0.35993	0.36083	0.35976	0.35974	0.36004	0.35874	0.35974	0.35976	0.35959
1	-0.00096	0.00044	-0.00057	0.00173	0.00017	-0.00063	-0.00052	-0.00026	0.00113	0.00032	0.00048	0.00023	0.00028
2	0.00028	-0.00076	0.00264	-0.00264	0.00024	0.00016	0.00084	-0.00040	0.00046	-0.00018	-0.00035	0.00019	-0.00004
3	-0.00167	-0.00115	-0.00028	-0.00112	-0.00002	0.00061	0.00075	0.00093	-0.00010	0.00116	-0.00063	0.00209	0.00001
4	-0.00033	0.00020	0.00037	-0.00113	0.00044	-0.00008	0.00051	-0.00007	0.00068	0.00143	0.00163	-0.00048	-0.00010
5	0.00007	-0.00003	-0.00070	0.00105	0.00169	0.00040	-0.00012	0.00071	0.00082	0.00075	0.00096	0.00101	0.00041
6	-0.00173	-0.00132	-0.00088	-0.00031	0.00124	0.00153	-0.00061	-0.00028	-0.00119	0.00064	-0.00003	-0.00020	-0.00008
7	-0.00094	0.00032	-0.00060	0.00140	-0.00009	0.00058	0.00049	-0.00004	-0.00155	0.00118	0.00090	-0.00017	0.00011
8	-0.00200	-0.00058	-0.00039	0.00027	-0.00101	0.00014	0.00107	-0.00007	0.00024	0.00065	-0.00043	-0.00173	-0.00010
9	-0.00108	-0.00096	0.00009	0.00017	-0.00064	0.00084	0.00011	-0.00129	-0.00049	-0.00015	-0.00068	0.00038	-0.00017
10	0.00031	-0.00017	0.00092	0.00031	0.00052	-0.00086	0.00046	-0.00141	-0.00189	-0.00004	0.00167	0.00099	-0.00010

Table 3 Variance-covariance matrices K_{CrCs} and K_{DrDs}

K_{CrCs}

	1,2	1,6	1,8	1,10	2,3	2,11
1,2	4.686	-0.087	0.062	2.478	0.213	-0.374
1,6	-0.087	0.967	0.996	-0.653	-0.083	0.021
1,8	0.062	0.996	3.057	1.372	0.564	-0.150
1,10	2.478	-0.653	1.372	1.868	0.262	0.207
2,3	0.213	-0.083	0.564	0.262	0.371	0.002
2,11	-0.374	0.021	-0.150	0.207	0.002	0.037

K_{DrDs}

	1,2	1,6	1,8	1,10	2,3	2,11
1,2	2.139	-0.331	0.248	-0.479	0.435	0.118
1,6	-0.331	6.067	2.475	0.325	0.767	-0.261
1,8	0.248	2.475	1.196	0.111	0.350	-0.080
1,10	-0.479	0.325	0.111	0.150	-0.088	-0.033
2,3	0.435	0.767	0.350	-0.088	0.224	-0.013
2,11	0.118	-0.261	-0.080	-0.033	-0.013	0.017